Physica A 443 (2016) 477–485

Contents lists available at ScienceDirect

Physica A

journal homepage: www.elsevier.com/locate/physa

Homogeneous cooling state of frictionless rod particles

S.M. Rubio-Largo [a,*], F. Alonso-Marroquin [b], T. Weinhart [c], S. Luding [c], R.C. Hidalgo [a]

[a] Department of Physics and Applied Mathematics, University of Navarra, 31080 Pamplona, Navarra, Spain
[b] School of Civil Engineering, The University of Sydney, Sydney NSW 2006, Australia
[c] Multi Scale Mechanics, CTW, UTwente, 7500 AE Enschede, Netherlands

HIGHLIGHTS

- A granular gas of rods has been simulated with DEM implemented on GPU.
- A homogeneous cooling state of frictionless 3D rods has been identified.
- Haff's Law is satisfied when introducing of a novel characteristic time.
- The energy equipartition between degrees of freedom has been clarified.

ARTICLE INFO

Article history:
Received 13 January 2015
Received in revised form 3 August 2015
Available online 9 October 2015

Keywords:
Granular systems
Homogeneous cooling
Rods
Numerical methods

ABSTRACT

In this work, we report some theoretical results on granular gases consisting of frictionless 3D rods with low energy dissipation. We performed simulations on the temporal evolution of soft spherocylinders, using a molecular dynamics algorithm implemented on GPU architecture. A homogeneous cooling state for rods, where the time dependence of the system's intensive variables occurs only through a global granular temperature, has been identified. We have found a homogeneous cooling process, which is in excellent agreement with Haff's law, when using an adequate rescaling time $\tau(\xi)$, the value of which depends on the particle elongation ξ and the restitution coefficient. It was further found that scaled particle velocity distributions remain approximately Gaussian regardless of the particle shape. Similarly to a system of ellipsoids, energy equipartition between rotational and translational degrees of freedom was better satisfied as one gets closer to the elastic limit. Taking advantage of scaling properties, we have numerically determined the general functionality of the magnitude $\mathcal{D}_c(\xi)$, which describes the efficiency of the energy interchange between rotational and translational degrees of freedom, as well as its dependence on particle shape. We have detected a range of particle elongations ($1.5 < \xi < 4.0$), where the average energy transfer between the rotational and translational degrees of freedom results greater for spherocylinders than for homogeneous ellipsoids with the same aspect ratio.

1. Introduction

Granular materials are commonly handled in everyday life and are involved in many industrial processes. For this reason, the study of their kinetic and mechanical properties is a very active research field [1,2]. Nevertheless, although these systems have been thoroughly examined in the past, they still reveal relevant and unexpected results [1,2].

* Corresponding author.
E-mail address: srubio.4@alumni.unav.es (S.M. Rubio-Largo).

http://dx.doi.org/10.1016/j.physa.2015.09.046
0378-4371/

Granular gases are very dilute systems of macroscopic grains, which move randomly loosing energy through inelastic collisions. Thus, in the absence of any external driving force, their energy uniformly decreases towards an homogeneous cooling state (HCS). In that condition, the time dependence of all its intensive variables results only from the global granular temperature [3,4]. For highly dissipative systems, however, the HCS rapidly becomes unstable and the system subsequently evolves into an inhomogeneous state where the cooling process notably slows down [5,6]. Consequently, the correlation between the particles' motion determines the rate of energy loss and large inhomogeneities in the density field are observed [5,7].

A number of theoretical studies have carefully analyzed particle–particle interactions during collision, explaining how inelasticity emerges from such interactions [8–10]. For soft grains, in which the repulsion force depends linearly on deformation, a constant restitution coefficient can be recovered [11,12] and, consequently, cooling kinetics following Haff's law would be expected. There is also experimental evidence of materials with variable restitution coefficients that depend on the relative velocity of the interacting particles. For instance, assuming nonlinear elastic repulsive forces (Hertzian contact) leads to a notably different algebraic decay of the system energy during the HCS [9].

On the other hand, in granular gases of spherical particles roughness leads to correlations between the translational and rotational degrees of freedom [13–15]. In general, both translational and rotational kinetic energies decrease with the same power law but differ from each other due to the breakdown of energy equipartition. Years ago, these correlations were quantified for a system of agitated rough spheres [16,17]. More recently, simulations of 3D gases of rough spheres shed light on the nontrivial process of energy interchange between the translational and rotational degrees of freedom, showing that the spin of a single grain can be correlated with the particle linear velocity [18,19].

The effect of particle shape on the kinetic evolution of granular gases has been studied by Aspelmeier and other researchers [20]. They developed a kinetic theory of hard needles based on the assumption of a homogeneous cooling state, in the very dilute limit. Hence, it was found that energy interchange between rotational and translational degrees of freedom is controlled by the macroscopic restitution coefficient and by the particle spatial distribution of mass. In recent years, there has been an increasing interest in the behavior of non-spherical grains both experimentally [21–26] and numerically [27–30]. Here, the primary interest is also focused on the evolution in time of the translational kinetic energy and rotational energy. Thus, it has been commonly found that in granular gases of elongated particles equipartition is not obeyed. Moreover, several details of the cooling process depend on particle aspect ratio, mass distribution of the grains and the driven mechanisms.

In the present work, we investigate the free cooling of a granular gas of elongated 3D particles, and both the role of inelasticity and the particle shape in the overall kinetic processes are analyzed. The paper is organized as follows: in Section 2 we introduce some basic concepts about the kinetics of granular gases, in Section 3 we described the numerical model and implementation of our algorithm, Section 4 discusses the results of the homogeneous cooling state of a system of frictionless rods. At the end, conclusions and outlook are drawn.

2. Homogeneous cooling state of rods

In a gas of spherical particles of radius a in HCS, the kinetic energy decreases homogeneously and the time evolution of all variables occurs only through their global temperature. By introducing the dimensionless translational temperature T and rotational temperature R as well as a characteristic time τ, Luding et al. [31] found that the kinetics of a granular gas of rough spheres is governed by the system of equations,

$$\begin{aligned} \frac{\mathrm{d}}{\mathrm{d}\tau}T &= -AT^{3/2} + BT^{1/2}R \\ \frac{\mathrm{d}}{\mathrm{d}\tau}R &= BT^{3/2} - CT^{1/2}R \end{aligned} \tag{1}$$

where A, B and, C are constants that depend on space dimensionality (see details in Ref. [31]). In 3D, $A = \frac{1-e_n^2}{4} + \eta(1-\eta)$, $B = \frac{\eta^2}{q}$ and $C = \frac{\eta}{q}\left(1 - \frac{\eta}{q}\right)$, where $\eta = \frac{q(1+e_t)}{(2q+2)}$ (in 3D $q = \frac{2}{5}$ for spheres) and e_n and e_t are the restitution coefficients in normal and tangential directions respectively. The equilibrium Enskog's collision rate for the initial temperature $T(0)$ reads as

$$G_{sph}(a) = 8(2a)^2 \frac{N}{V}\sqrt{\frac{\pi}{m}} g(2a) T^{1/2}(0) \tag{2}$$

where N is the number of particles per unit of volume, m and V are the mass and volume of the particles, respectively.

This variable is commonly used to rescale time according to $\tau = \frac{2}{D} G_{sph} t$, where D accounts for the number of translational degrees of freedom. It has been found that in general the principle of equipartition does not necessarily apply, resulting asymptotically in $T_{tr}(\tau)/T_{rot}(\tau) \neq 1$.

The HCS of systems consisting of frictionless oblate and prolate ellipsoids has been recently examined [27,28]. There, it was introduced a granular temperature $T_{tot}(t)$ of the gas as a weighted average of $T_{tr} = \frac{2}{3N}\sum_{i=1}^{N} \frac{1}{2} m v_i^2$ and

$T_{rot} = \frac{1}{N}\sum_{i=1}^{N}\frac{1}{2}I\omega_i^2$ with the weights given by the respective degrees of freedom:

$$T_{tot}(t) = \frac{3}{5}T_{tr}(t) + \frac{2}{5}T_{rot}(t). \tag{3}$$

Villemot and Talbot [27] found that for a gas of frictionless elongated elastic ellipsoids the principal of equipartition holds [27] and, accordingly, the energy stored in the rotational $T_{rot}(t)$ and translational $T_{tr}(t)$ degrees of freedom equally evolve in time, tending asymptotically towards $T_{tr}(t)/T_{rot}(t) \approx 1$. They also observed that T_{tot} followed Haff's Law [32]

$$\frac{T_{tot}(\tau)}{T_{tot}(0)} = \frac{1}{(1+\tau)^2}, \tag{4}$$

when choosing an appropriate time scale $\tau = \alpha G_{ellip} t$, where $\alpha = \frac{1-e_n^2}{2D}$ and $D = 5$ was interpreted as the total number of degrees of freedom among which energy is transferred [27]. Moreover, the collision frequency G_{ellip} was analytically derived [27]. Those results motivated us to examine the HCS of dissipative frictionless rods.

Assuming the existence of a HCS for frictionless rods, one may argue that the mean field scheme may also apply to a dilute gas of rods. Again the energy lost can be entirely described by the particles restitution coefficient e_n and the evolution of the granular temperature would obey Eq. (4). Hence, for the cooling dynamics of rods, we propose a new characteristic time, $\tau = \alpha G_{rd} t = \alpha \mathcal{D}_c G_{sph} t$, which is written in terms of the collision frequency G_{sph} of a sphere with the same volume. Note that $\mathcal{D}_c$ measures the average energy transfer between rotational and translational degrees of freedom due to collisions. As we pointed out earlier, for ellipsoids there is an analytical expression of G_{ellip} [27], but for rods this analytic description remains unrevealed. In this paper, we take advantage of the homogeneous properties of the HCS of rods to numerically find the functionality of $\mathcal{D}_c$, according to the particle elongation.

3. Numerical model

We have developed a hybrid GPU–CPU discrete element algorithm for simulating three-dimensional spherocylinders. The present implementation is based on a similar algorithm of rough spheres [33] that has been recently introduced in CUDA (Computer Unified Device Architecture), which is a parallel computing platform by NVIDIA [34]. The application developed, as most GPGPU software, has a heterogeneous architecture. This means that some pieces of code run on the CPU and others on the GPU.

In the model, the rods are considered as sphero-cylinders, which are characterized by their length l and sphero-radius r. Thus, it aspect ratio is defined by $\xi = (l + 2r)/2r$. For calculating the contact interaction, $\vec{F}_{ij}$, we use an efficient algorithm proposed by Alonso-Marroquín et al. [35,36], allowing the simulation of a large number of particles. This numerical method is based on the concept of spheropolygons, i.e., a polygon i is defined by the set of vertices V_i and edges E_i. A spherocylinder is the simplest spheropolyhedron and it has two vertices and one edge, thus the contact detection between to spherocylinders is reduced to find the closer point between two segments. Afterwards, two imaginaries spheres can be drawn on each spherocylinder. Thus, the interaction is equivalent to the inter-penetration between the two neighboring spheres of radius r. Thus, the force $\vec{F}_{ij}$ exerted on particle i by the particle j is defined by: $\vec{F}_{ij} = -\vec{F}_{ji}$. Hence, the local interaction between two particles in contact is only governed by the overlap distance δ between two segments. The force $\vec{F}_{ij}$ can be decomposed as $\vec{F}_{ij} = F^N \cdot \vec{n} + F^T \cdot \vec{t}$, where F^N is the component in normal direction $\vec{n}$ to the contact plane. Complementary, F^T is the component of the force in the tangential direction $\vec{t}$. To define the normal interaction F^N, we use a linear elastic force proportional to the overlap distance δ. Fig. 1(a) illustrates the sketch of the interaction between two spherocylinders. The corresponding neighboring spheres have been highlighted as well as the normal and tangential directions. To account for dissipation, a velocity dependent viscous damping is assumed. Hence, the total normal force reads: $F^N = -k^N\delta - \gamma^N m_r v_{rel}^N$, where k^N is the spring constant in the normal direction, $m_r = \frac{m_i m_j}{(m_i+m_j)} = \frac{m}{2}$ stands for the pair's reduced mass, γ^N is the damping coefficient in the normal direction and v_{rel}^N is the normal relative velocity between i and j. The tangential force F^T also contains an elastic term and a tangential frictional term accounting for static friction between the grains. Taking into account Coulomb's friction constrain, which reads as, $F^T = \min\{-k^T\xi - \gamma^T m_r \cdot |v_{rel}^T|,\ \mu F^N\}$, where γ^T is the damping coefficient in tangential direction, v_{rel}^T is the tangential component of the relative contact velocity of the overlapping pair. The variable ξ represents the elastic elongation of an imaginary spring with k^T at the contact [37]. The elongation increases or decreases according to $\frac{d\xi(t)}{dt} = v_{rel}^T$ depending on the overlap distance between the interacting particles [37,38]. Here, μ is the friction coefficient of the particles. Although the implementation is already generalized for frictional particles, below we will only refer to non-frictional cases.

The Newton's equation of motion for rods particles i is given by,

$$\sum_{j=1}^{N_c}\vec{F}_{ij} = m\ddot{\vec{r}}_i \tag{5}$$

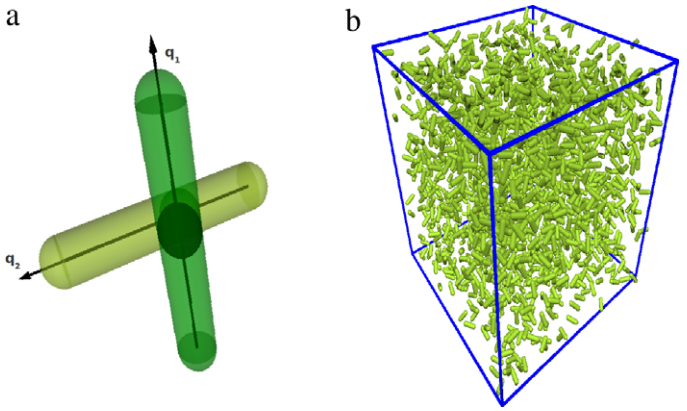

Fig. 1. In (a) Sketch of the interaction among two particles is shown; In (b) Partial snapshot of a system of 32 768 spherocylinders with elongation of $\xi = 3$. Volume fraction of $\eta_r = 0.045$.

for the translation degrees of freedom. The *Euler*'s equations describe the rotational motion,

$$\begin{aligned}
\sum_{j=1}^{N_c} \tau_{ij}^{x} &= M_i^x = I_{xx}\,\dot{\omega}_i^x - (I_{yy} - I_{zz})\,\omega_i^y\,\omega_i^z \\
\sum_{j=1}^{N_c} \tau_{ij}^{y} &= M_i^y = I_{yy}\,\dot{\omega}_i^y - (I_{zz} - I_{xx})\,\omega_i^z\,\omega_i^x \\
\sum_{j=1}^{N_c} \tau_{ij}^{z} &= M_i^z = I_{zz}\,\dot{\omega}_i^z - (I_{xx} - I_{yy})\,\omega_i^x\,\omega_i^y .
\end{aligned} \tag{6}$$

In these expressions, m represents the mass of the particle and I_{xx}, I_{yy}, I_{zz} are the eigen-values of the moment of inertia tensor I_{ij}. $\mathbf{F}_{ij}$ is the force exerted by particle j on particle i and τ_{ij} accounts for its corresponding torque τ_{ij}. The total force $\mathbf{F_i}$, and momentum $\mathbf{M_i}$ acting on particle i are obtained as sums of the pair-wise interaction of particle i with its contacting neighbors.

We developed CUDA-thrust function integrators, for both the translation and the rotational degree of freedom. To integrate the 3D translational equations of motion a Verlet-velocity numerical algorithm was implemented. The CUDA-thrust functions/methods are called by the host(CPU), inside the Molecular Dynamic loop. Hence, all particles positions and velocities are calculated in parallel.

The numerical implementation of the rotational degree of freedom deserves a more detailed description. The set of Eq. (6) describes the evolution of the particles angular velocity ω, in the body frame. Additional equations are necessary to describe the evolution of the particle orientation. Here, we adopted the quaternion representation, which has several demonstrated technical advantages over other methods [39]. The unit quaternion $q = (q_0, q_1, q_2, q_3) = q_0 + q_1 i + q_2 j + q_3 k$ characterizes the particle orientation [40,41] where $\sum_{i=0}^{3} q_i^2 = 1$. Each quaternion variable satisfies the rotational equation of motion [40,41]

$$\dot{q} = \frac{1}{2} Q(q)\omega \tag{7}$$

where

$$\dot{q} = \begin{pmatrix} \dot{q}_0 \\ \dot{q}_1 \\ \dot{q}_2 \\ \dot{q}_3 \end{pmatrix}, \qquad Q(q) = \begin{pmatrix} q_0 & -q_1 & -q_2 & -q_3 \\ q_1 & q_0 & -q_3 & q_2 \\ q_2 & q_3 & q_0 & -q_1 \\ q_3 & -q_2 & q_1 & q_0 \end{pmatrix}, \qquad \omega = \begin{pmatrix} 0 \\ \omega_x \\ \omega_y \\ \omega_z \end{pmatrix}.$$

Eqs. (6) and (7) are solved using a Fincham's leap-frog algorithm [42]. The approach obtains $q(t+\mathrm{d}t)$ from $q(t)$ using equation

$$q(t + \mathrm{d}t) = q(t) + \mathrm{d}t\,\dot{q}(t) + \frac{\mathrm{d}t^2}{2}\ddot{q}(t) + O(\mathrm{d}t^3) = q(t) + \mathrm{d}t\,\dot{q}\left(t + \frac{\mathrm{d}t}{2}\right) + O(\mathrm{d}t^3). \tag{8}$$

Hence, quaternion derivative at mid-step $\dot{q}(t + \mathrm{d}t/2)$ is required. Eqs. (7) indicates that $q(t + \mathrm{d}t/2)$ and $\omega(t + \mathrm{d}t/2)$ are required, the former can be easily calculated using

$$q\left(t + \frac{\mathrm{d}t}{2}\right) = q(t) + \dot{q}(t)\frac{\mathrm{d}t}{2} \tag{9}$$

where $\dot{q}(t)$ is again obtained from (7), prior to which $\omega(t)$ can be calculated using

$$\omega_x(t) = \omega_x\left(t - \frac{\mathrm{d}t}{2}\right) + \left[\frac{I_{yy} - I_{zz}}{I_{xx}}\,\omega_y\left(t - \frac{\mathrm{d}t}{2}\right)\omega_z\left(t - \frac{\mathrm{d}t}{2}\right) + \frac{M^x}{I_{xx}}\right]\frac{\mathrm{d}t}{2} \tag{10}$$

$$\omega_y(t) = \omega_y\left(t - \frac{\mathrm{d}t}{2}\right) + \left[\frac{I_{zz} - I_{xx}}{I_{yy}}\,\omega_z\left(t - \frac{\mathrm{d}t}{2}\right)\omega_x\left(t - \frac{\mathrm{d}t}{2}\right) + \frac{M^y}{I_{yy}}\right]\frac{\mathrm{d}t}{2} \tag{11}$$

$$\omega_z(t) = \omega_z\left(t - \frac{\mathrm{d}t}{2}\right) + \left[\frac{I_{xx} - I_{yy}}{I_{zz}}\,\omega_x\left(t - \frac{\mathrm{d}t}{2}\right)\omega_y\left(t - \frac{\mathrm{d}t}{2}\right) + \frac{M^z}{I_{zz}}\right]\frac{\mathrm{d}t}{2} \tag{12}$$

in the same way $\omega\left(t + \frac{\mathrm{d}t}{2}\right)$, is determined as,

$$\omega_x\left(t + \frac{\mathrm{d}t}{2}\right) = \omega_x\left(t - \frac{\mathrm{d}t}{2}\right) + \left[\frac{I_{yy} - I_{zz}}{I_{xx}}\,\omega_y\left(t - \frac{\mathrm{d}t}{2}\right)\omega_z\left(t - \frac{\mathrm{d}t}{2}\right) + \frac{M^x}{I_{xx}}\right]\mathrm{d}t \tag{13}$$

$$\omega_y\left(t + \frac{\mathrm{d}t}{2}\right) = \omega_y\left(t - \frac{\mathrm{d}t}{2}\right) + \left[\frac{I_{zz} - I_{xx}}{I_{yy}}\,\omega_z\left(t - \frac{\mathrm{d}t}{2}\right)\omega_x\left(t - \frac{\mathrm{d}t}{2}\right) + \frac{M^y}{I_{yy}}\right]\mathrm{d}t \tag{14}$$

$$\omega_z\left(t + \frac{\mathrm{d}t}{2}\right) = \omega_z\left(t - \frac{\mathrm{d}t}{2}\right) + \left[\frac{I_{xx} - I_{yy}}{I_{zz}}\,\omega_x\left(t - \frac{\mathrm{d}t}{2}\right)\omega_y\left(t - \frac{\mathrm{d}t}{2}\right) + \frac{M^z}{I_{zz}}\right]\mathrm{d}t. \tag{15}$$

To avoid build-up errors, the quaternions $q(t)$ are renormalized every time step [43]. The angular integrators have also been implemented as CUDA-thrust functions. As we pointed out earlier, those kernels run on the GPU device allowing the evaluation of the spatial and angular positions of a block of particles, with a double precision accuracy in a single computational time step.

The parameters of the contact model are chosen as follows: to model hard particles the maximum overlap must always be much smaller than the particle size. This has been ensured by introducing values for normal elastic constant, $k_n = 2.8 \times 10^6$ N/m and density $\rho = 2600$ kg/m^3. To compare the numerical simulations with existing analytical predictions of kinetic theory, systems of rods with contact parameters equivalent to restitution coefficients $e_n = 0.88,\ 0.90,\ 0.96$ were studied. Thus, the normal dissipation parameter γ_n was calculated using the normal coefficient of restitution e_n by the equation $\gamma_n = \sqrt{(4k_n m_{12})/((\frac{\pi}{\ln 1/e_n})^2 + 1)}$ and for frictionless rods we have set $\gamma_t = 0$ and $k_t = 0$. The collision time can be estimated $t_c = \pi\sqrt{m_{12}/k_n}$ and, accordingly, a time step $\Delta t = t_c/50$ have been used.

It is important to indicate that the assumption of a constant restitution e_n is not totally valid when using DEMs of non-spherical particles, due the energy losing depends on the collision details. In the discussion of the results, we introduce a way to overcome this situation when comparing the numerical data with its corresponding analytical prediction.

4. Simulation results

We have numerically studied the free cooling kinetics of a dilute granular gas of rods. In all simulations reported here, a fixed number of particles $N = 2^{15} = 32\,768$ confined in a square box of size $L = 2$ meters are used. Simulations are computed using rods of different aspect ratios, from $\xi = 1.0$ to $\xi = 4.0$, with $\xi = (l + 2r)/2r$ but always keeping the packing fraction equal to $\eta_r = 0.045$, particle volume $V_p = \eta_r L^3/N$ and mas $m = \rho V_p$. In each case, the values of r and l are adjusted to the choice of η_r and ξ. Initially, the particles are homogeneously distributed in space and their translational and rotational velocities followed a uniform Gaussian distribution in each direction. Moreover, with the aim of avoiding the initial configuration effects, dissipation is initially disabled, and a number of time steps without energy dissipation are performed. Afterwards, the energy loss is enabled and the main loop of the program is executed. To avoid wall effects periodic boundary conditions were implemented. The simulations run until the total mean translational and rotational kinetic energies decayed several orders of magnitude. In Fig. 1(b) we display a snapshot of the simulated system with $\xi = 2$.

The dynamics of freely evolving gases of rods were examined by monitoring the temporal evolution of the mean translational $T_{tr}(t)$ and rotational $T_{rot}(t)$ kinetic energies, which are usually referred as granular temperatures. In Fig. 2(a), the evolution of the translational kinetic energy $T_{tr}(t)$ in time is presented. In similarity to spherical particles, a gas of rods cools down uniformly. As it was expected due to the low dissipation, in all cases the system seems to evolve to a HCS where the granular temperature asymptotically decreases following Haff's law t^{-2}. However, the cooling dynamics are notably accelerated for elongated particles. In Fig. 2(b), the asymptotic ratio of T_{tr}/T_{rot} is examined varying the elongation and the coefficient of normal restitution. Note that one observes two regions, in the case of short rods $\xi < 1.5$ the translational degree of freedom cools down faster than the rotational one $T_{tr}/T_{rot} < 1$. For longer rods, however, energy equipartition is better satisfied, $T_{tr}/T_{rot} \approx 1$, especially as one gets closer to the elastic limit $e_n = 1$. This indicates that for short rods, the energy interchange between degrees of freedom is notably altered and conditions of total energy equipartition are not satisfied. One could argue that below values of $\xi_c \approx 1.5$ a single collision of two particles may favor the translational to rotational energy transfer. Note that where the contact point is close to the center of mass of one of the particles, its

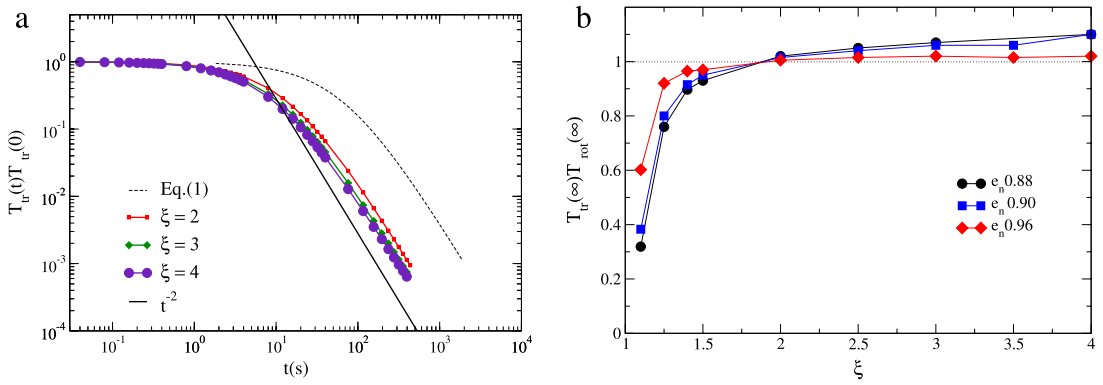

Fig. 2. In (a) the evolution of the kinetic energy of several systems of rods with $e_n = 0.88$. For comparison, it is shown the theoretical result corresponding to the numerical solution in real time of Eq. (1) with similar volume fraction and tangential restitution coefficient $e_t = 1$; in (b) the ratios between the translational and rotational kinetic energy T_{tr}/T_{rot}, at very long times are also shown.

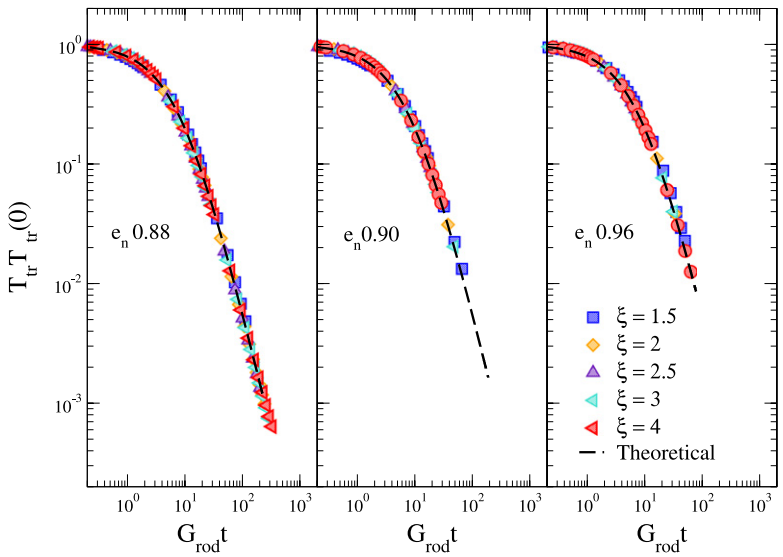

Fig. 3. The collapse of the curves $T_{tr}/T_{tr}(0)$ vs. $G_{rd}t = \mathcal{D}_c(\xi)G_{sph}t$ for each e_n is illustrated. The analytical values of G_{sph} have been calculated using Eq. (2), for equivalent spheres with the same volume V_p.

translational energy diminishes, while its rotational degree of freedom is less affected. When particles are shorter, central collisions are more and more frequent, which may unbalance the energy interchange process. This behavior has also been observed in granular gases of monodisperse ellipsoids [27]. It is important to remark that for $\xi = 1.0$ is singular due to the abrupt absence of torques and rotational degrees of freedom. Note that for frictionless spheres the rotational degrees of freedom are completely decoupled from the dynamical evolution of the gas. Moreover, the energy equipartition is also lost when the dissipation is enhanced, we could argue that the numerical performance of the algorithm might be conditioned by the hardness of the used particle.

In Fig. 3 the time evolution of the kinetic translational energy is compared to the mean field analytical results, which are available for a gas of spheres with similar macroscopic properties [31]. The time scale has been rescaled with its corresponding geometrical factor, resulting a collision frequency, $G_{rd} = \mathcal{D}_c(\xi)G_{sp}$. Note that the only free parameter is $\mathcal{D}_c(\xi)$, which has been used as fitting parameter comparing our simulations to the analytical prediction of Eq. (1) for the same volume fraction $\eta_r = 0.045$, particle mass and frictionless particles $e_t = 1$. It is remarkable that all curves with different aspect ratios collapse into the analytical prediction. This proves the existence of a HCS, where the total energy of the system homogeneously decreases and the time evolution of all variables can be described only through its global granular temperature.

Then we can go one step forward to test whether the nature of the system kinetics is independent of the dissipation parameters. In Fig. 4, we illustrate how Haff's Law Eq. (4) in a time scale $\tau(\xi)$ applies to the homogeneous cooling state of rods in a wide regime of elongations. The solid line corresponds to the theoretical approximation of $T_{tot}(\tau)$; the chosen time scale $\tau(\xi)$ is explained in the next paragraph. The scaling of the curves and the remarkable agreement with the analytical formula

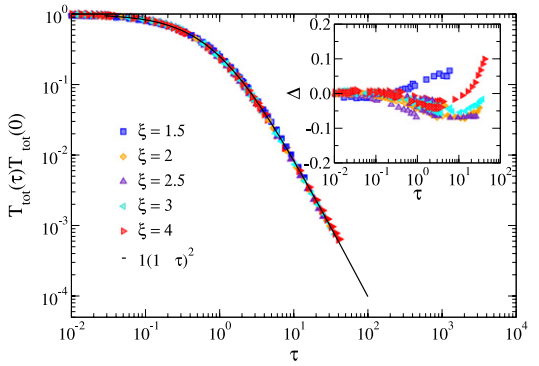

Fig. 4. Evolution of the total temperature $T_{tot}(\tau)/T_{tot}(0)$ vs. the characteristic time τ, note the scaling of all the curves when using the characteristic time $\tau(\xi) = \alpha^* \mathcal{D}_c(\xi) G_{sp} t$, numerical data corresponding to several particles elongations $d > 1.5$ and restitution coefficients ($e_n = 0.88; 0.90; 0.96$) have been included. Similarly to the case of ellipsoids [28] and effective dissipation factor $\alpha^* = \sqrt{3/2}\alpha$ have been used [29]. The inset represents the evolution in time of the quality factor $\Delta = \frac{T_{tot} - T_{th}}{T_{th}}$.

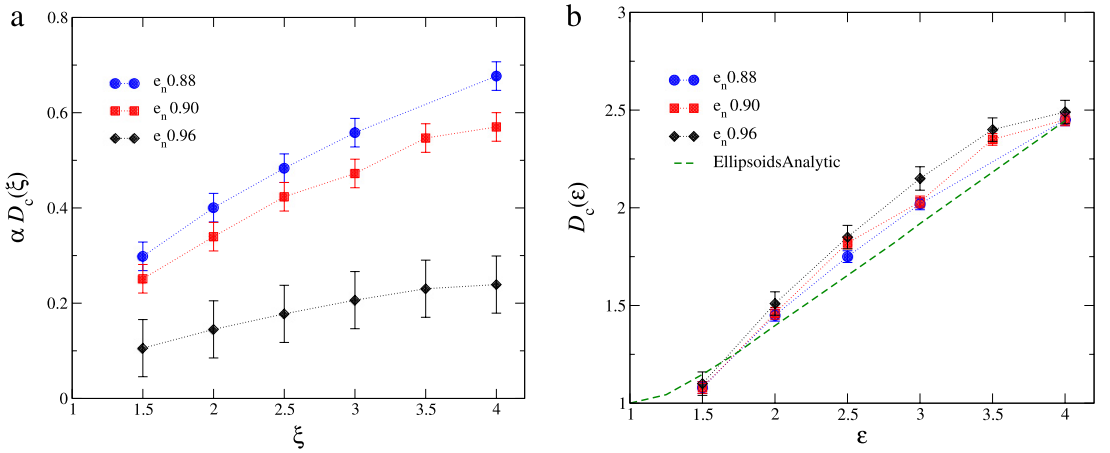

Fig. 5. Numerical estimation of $\alpha \mathcal{D}_c(\xi)$ (a) and the corresponding $\mathcal{D}_c(\xi)$ (b) as a function of the elongation, obtained collapsing each numerical data for the translational kinetic energy and its corresponding analytic prediction. For comparison in (b) the dashed line corresponds to the theoretical result for homogeneous ellipsoids given in Ref. [27].

indicate the presence of a homogeneous cooling process, in similarity to spheres with constant restitution coefficient. In the inset of Fig. 4, the values of the scaling quality factor $\Delta(\tau) = \frac{T_{tot} - T_{th}}{T_{th}}$, where $T_{th}(\tau) = \frac{1}{(1+\tau)^2}$ are shown. The outcomes indicate that the error is practically smaller than the 10% in all cases. However, the scaling resulted in lower accuracy for longer times and highly dissipative systems due to the imminent development of clustering and a non-homogeneous cooling dynamics. The consistency of our results validate the performance of the hybrid numerical algorithm running on GPU architecture.

It is important to mention that the cooling dynamics predicted by Eq. (4) is based on the assumption that the restitution coefficient is constant, regardless the details of the collision event. This presumption is natural when performing event-driven simulations and DEM of hard spherical particles. Assuming a constant restitution coefficient is not totally valid when using DEMs of non-spherical particles, because the energy losing generally depends on the type of collision. Nevertheless, in very dilute systems it is plausible to consider only binary collision and the energy lost can be entirely described by an effective dissipation. In Ref. [28], the cooling dynamics of frictionless ellipsoids using DEM was explored and the results were also compared to Haff's law Eq. (4) in a time scale $\tau(\xi) = \alpha^* G_{ellip}(\xi) t$ where $G_{ellip}(\xi)$ was analytically deduced [27]. Note that full agreement with the analytic formula Eq. (4) was only found identifying α^* with an effective dissipation coefficient $\alpha^* = \sqrt{3/2}\,\alpha$. Having said that, here we also used a characteristic time $\tau = \alpha^* G_{rd}(\xi) t$ and take advantage of the homogeneous properties of the HCS of rods to numerically find the functionality of $G_{rd}(\xi)$ in terms of G_{sph}, $\tau = \alpha^* \mathcal{D}_c(\xi) G_{sph} t$.

Fig. 5(a)–(b) shows the values of $\alpha \mathcal{D}_c(\xi)$ and $\mathcal{D}_c(\xi)$ obtained from the direct scaling with Haffs law. The procedure allows us to numerically determine the functionality of $\mathcal{D}_c(\xi)$, which quantifies the efficiency of the energy transfer between rotational and translation degrees of freedom, as well as its particle size dependence. For comparison, we also included in Fig. 5(b) data corresponding to the analytic outcomes obtained for frictionless monodisperse ellipsoids [27]. It is important to remark that even though using rods and ellipsoids with the same volume, still both geometrical shapes have different

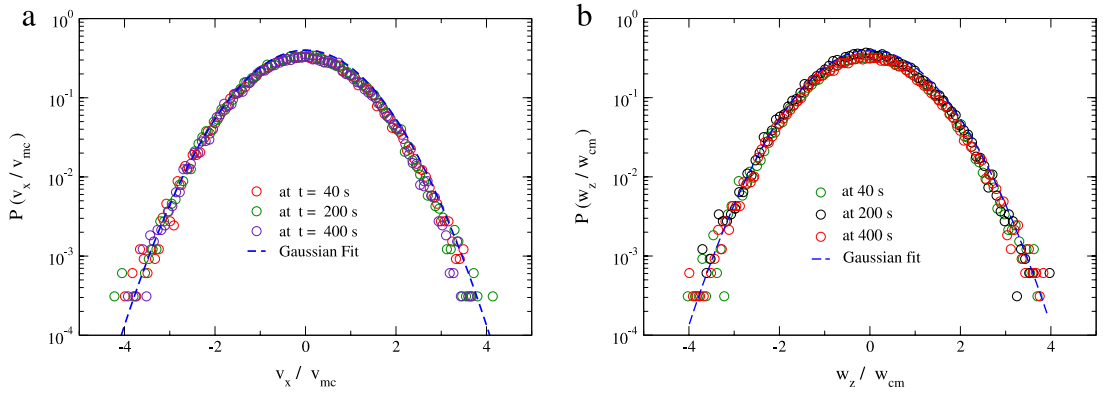

Fig. 6. In (a) velocity distributions and in (b) angular velocity distributions obtained for a systems of frictionless rods. Results for $\xi_n = 0.88$ at $t = 40, 200,$ 400 s. The dashed lines correspond to a Gaussian fits.

average surface area $\mathcal{S}c(\xi)$. Consequently, one would have to compare the magnitude $\mathcal{D}_c(\xi)\mathcal{S}c(\xi)$. For sake of simplicity, the analytic values $\mathcal{D}_c(\xi)\mathcal{S}c_{ellip}(\xi)$ of Ref. [27] have been rescaled with $\mathcal{S}c_{sph}$, the average surface of its corresponding sphere with the same volume. Thus, the comparison is done with $\mathcal{D}_c(\xi)\mathcal{S}c_{ellip}(\xi)/\mathcal{S}c_{sph}$ and, as it can be expected, the results for rods are very close to the outcomes for ellipsoids with similar elongations. In spite of that, there is a region where the rods and ellipsoids behaved slightly different. It is noticeable that for $(1.5 < \xi < 4.0)$ the average energy transfer per unit of area between the rotational and translational degrees of freedom resulted slightly greater for rods than ellipsoids with similar elongation.

During the cooling process both, linear and angular, velocity statistics are also examined. The simulation begins from a uniform velocity distribution for both, the translational and angular degrees of freedom. Before starting to analyze the system temporal evolution, the system is allowed to execute several hundreds of collisions without dissipation. Note that due the low dissipation, particles cool down uniformly over a wide range of time. Thus, all the temporal dependences are calculated through the mean values of the translational and rotational temperature. The velocity distributions at different snapshot of the simulation are shown in Fig. 6(a). In all cases, the velocity distributions is close to a Gaussian distribution $P(v_i) = \frac{1}{\sigma_v\sqrt{2\pi}}e^{-v_i^2/2\sigma_v^2}$. For the rotational degree of freedom, in Fig. 6(b) we plot the angular velocity distribution for each angular component obtained at different times. The data proves that cooling process at the rotational level also occurs homogeneously. Thus, the two components of the angular velocity behave equivalently and with the same characteristic values. In all cases the distribution follows a Gaussian behavior $P(w_i) = \frac{1}{\sigma_w\sqrt{2\pi}}e^{-w_i^2/2\sigma_w^2}$ featuring the expected homogeneous cooling process, regardless of the particle anisotropy. Nevertheless, the limitation of our system size N prevents us from analyzing the tails of the distributions, where deviations from the Gaussian behavior may appear [44].

Conclusions and outlook: We have introduced a hybrid CPUGPU implementation of an accurate molecular dynamics algorithm of a system of 3D spherocylinders. We further have numerically described a homogeneous cooling state of a granular gas consisting of 3D spherocylindrical particles. In that state, the evolution of the systems, intensive variables occurs only through a global granular temperature that sets the relevant time-scale. We examined the uniform cooling kinetics and introduced a rescaled time $\tau(\xi)$, which depends on the particle elongation. Excellent agreement with Haff's law and energy equipartition are observed for elongated particles with $\xi > 1.5$. The agreement is enhanced when approaching the elastic limit. Taking advantage of scaling properties, we have numerically determined the general functionality of the quantity $\mathcal{D}_c(\xi)$, which describes the efficiency of the energy interchange between rotational and translational degrees of freedom, as well as its dependence with the particle shape. When the cooling process is explored at very large time scales or when examining higher dissipative systems, we observe deviations from Haffs law Eq. (4). In those cases, the system evolves into an inhomogeneous state where the cooling dynamics notably slows down. Moreover, strong inhomogeneities in the velocity field and clustering are present. In this regime the collective motions of particles determine the process dynamics and is very difficult to describe analytically. Finally, we have also implemented rough generalized rods and particle friction was found to have a significant influence on system cooling kinetics. In that case, the azimuthal and polar rotational degrees independently evolve and only correlate with the translational degrees of freedom at very long time. These issues will be investigated in future works.

Acknowledgments

The Spanish MINECO (Projects FIS2011-26675 and FIS2014-57325), the University of Navarra (PIUNA Program) and the University of Sydney Civil Engineering Research Development Scheme (CERDS) have supported this work. S.M. Rubio-Largo thanks Asociación de Amigos de la Universidad de Navarra. We thank D. Hanaor for proof-reading the manuscript.

References

[1] I. Aranson, L. Tsimring, Patterns and collective behavior in granular media: Theoretical concepts, Rev. Modern Phys. 78 (2006) 641.
[2] T. Pöschel, T. Schwager, Computational Granular Dynamics, Springer-Verlag, Berlin, 2005.
[3] J. Brey, M. Ruiz-Montero, D. Cubero, Homogeneous cooling state of a low-density granular flow, Phys. Rev. E 54 (1996) 3664.
[4] V. Garzó, J. Dufty, Homogeneous cooling state for a granular mixture, Phys. Rev. E 60 (5) (1999) 5706–5713.
[5] S. Miller, S. Luding, Cluster growth in two- and three-dimensional granular gases, Phys. Rev. E 69 (2004) 031305.
[6] X. Nie, E. Ben-Naim, S. Chen, Dynamics of freely cooling granular gases, Phys. Rev. Lett. 89 (20) (2002) 204301. e-print cond-mat/0209412.
[7] A. Puglisi, V. Loreto, U.M.B. Marconi, A. Petri, A. Vulpiani, Clustering and non-Gaussian behavior in granular matter, Phys. Rev. Lett. 81 (18) (1998) 3848–3851.
[8] T. Schwager, Coefficient of restitution for viscoelastic disks, Phys. Rev. E 75 (2007) 051305.
[9] N. Brilliantov, T. Pöschel, Velocity distribution in granular gases of viscoelastic particles, Phys. Rev. E 61 (2000) 5573.
[10] M. Shinde, D. Das, R. Rajesh, Equivalence of the freely cooling granular gas to the sticky gas, Phys. Rev. E 79 (2009) 021303.
[11] N. Brilliantov, F. Spahn, J. Hertzsch, T. Pöschel, Model for collisions in granular gases, Phys. Rev. E 53 (5) (1996) 5382.
[12] S. Luding, Collisions & contacts between two particles, in: H.J. Herrmann, J.-P. Hovi, S. Luding (Eds.), Physics of Dry Granular Media, in: NATO ASI Series E, vol. 350, Kluwer Academic Publishers, Dordrecht, 1998, pp. 285–304.
[13] K. Nichol, K.E. Daniels, Equipartition of rotational and translational energy in a dense granular gas, Phys. Rev. Lett. 108 (2012) 018001.
[14] A. Sack, M. Heckel, J.E. Kollmer, F. Zimber, T. Pöschel, Energy dissipation in driven granular matter in the absence of gravity, Phys. Rev. Lett. 111 (2013) 018001.
[15] Y. Grasselli, G. Bossis, R. Morini, Translational and rotational temperatures of a 2D vibrated granular gas in microgravity, Eur. Phys. J. E 38 (2015) 8.
[16] R. Cafiero, S. Luding, H. Herrmann, Two-dimensional granular gas of inelastic spheres with multiplicative driving, Phys. Rev. Lett. 84 (2000) 6014–6017.
[17] R. Cafiero, S. Luding, H. Herrmann, Rotationally driven gas of inelastic rough spheres, Europhys. Lett. 60 (2002) 854.
[18] N.V. Brilliantov, T. Pöschel, W.T. Kranz, A. Zippelius, Translations and rotations are correlated in granular gases, Phys. Rev. Lett. 98 (2007) 128001.
[19] W. Kranz, N. Brilliantov, T. Pöschel, A. Zippelius, Correlation of spin and velocity in the homogeneous cooling state of a granular gas of rough particles, Eur. Phys. J. Spec. Top. 179 (1) (2009) 91–111.
[20] T. Aspelmeier, G. Giese, A. Zippelius, Cooling dynamics of a dilute gas of inelastic rods: A many particle simulation, Phys. Rev. E 57 (1998) 857.
[21] A. Kudrolli, G. Lumay, D. Volfson, L. Tsimring, Swarming and swirling in self-propelled polar granular rods, Phys. Rev. Lett. 100 (2008) 058001.
[22] T. Kanzaki, M. Acevedo, I. Zuriguel, I. Pagonabarraga, D. Maza, R.C. Hidalgo, Stress distribution of faceted particles in a silo after its partial discharge, Eur. Phys. J. E 34 (2011) 133.
[23] T. Börzsönyi, B. Szabó, G. Törös, S. Wegner, J. Török, E. Somfai, T. Bien, R. Stannarius, Orientational order and alignment of elongated particles induced by shear, Phys. Rev. Lett. 108 (2012) 228302.
[24] K. Harth, U. Kornek, T. Trittel, U. Strachauer, S. Höme, K. Will, R. Stannarius, Granular gases of rod-shaped grains in microgravity, Phys. Rev. Lett. 110 (2013) 144102.
[25] M. Acevedo, R.C. Hidalgo, I. Zuriguel, D. Maza, Influence of the feeding mechanism on deposits of square particles, Phys. Rev. E 87 (2012) 012202.
[26] S. Wegner, R. Stannarius, A. Boese, G. Rose, B. Szabo, E. Somfai, T. Borzsonyi, Effects of grain shape on packing and dilatancy of sheared granular materials, Soft Matter 10 (2014) 5157–5167.
[27] F. Villemot, J. Talbot, Homogeneous cooling of hard ellipsoids, Granular Matter 14 (2) (2012) 91–97.
[28] S.M. Rubio-Largo, P. Lind, D. Maza, R.C. Hidalgo, Granular gas of ellipsoids: analytical collision detection implemented on GPUs, Comput. Part. Mech. 2 (2015) 127–138.
[29] G. Costantini, U. Marini Bettolo Marconi, G. Kalibaeva, G. Ciccotti, The inelastic hard dimer gas: a nonspherical model for granular matter, J. Chem. Phys. 122 (16) (2005) 164505.
[30] T. Kanzaki, R. Hidalgo, D. Maza, I. Pagonabarraga, Cooling dynamics of a granular gas of elongated particles, J. Stat. Mech. 2010 (2010) P06020.
[31] S. Luding, M. Huthmann, S. McNamara, A. Zippelius, Homogeneous cooling of rough dissipative particles: Theory and simulations, Phys. Rev. E 58 (1998) 3416–3425.
[32] P. Haff, Grain flow as a fluid-mechanical phenomenon, J. Fluid Mech. 134 (1983) 401–430.
[33] R.C. Hidalgo, T. Kanzaki, F. Alonso-Marroquin, S. Luding, On the use of graphics processing units (GPUs) for molecular dynamics simulation of spherical particles, AIP Conf. Proc. 1542 (1) (2013) 169–172.
[34] S. Green, Particle simulation using cuda, Tech. rep, NVIDIA Coorporation, Santa Clara, USA, 2010.
[35] F. Alonso-Marroquín, Spheropolygons: A new method to simulate conservative and dissipative interactions between 2D complex-shaped rigid bodies, Europhys. Lett. 83 (2008) 14001.
[36] F. Alonso-Marroquín, Y. Wang, An efficient algorithm for granular dynamics simulations with complex-shaped objects, Granular Matter 11 (2009) 317–329.
[37] P. Cundall, O. Strack, A discrete numerical model for granular assemblies, Geotechnique 29 (1979) 47–65.
[38] G. Duvaut, J.-L. Lions, Les Inéquations en Mécanique et en Physique, Dunod, Paris, 1972.
[39] J. Kuipers, Quaternions and Rotation Sequences: A Primer with Applications to Orbits, Aerospace, and Virtual Reality, Princeton University Press, 2002.
[40] D. Evans, On the representation of orientation space, Mol. Phys. 34 (1977) 317–325.
[41] D. Evans, S. Murad, Singularity free algorithm for molecular dynamic simulation of rigid polyatomice, Mol. Phys. 34 (1977) 327–331.
[42] D. Fincham, Leapfrog rotational algorithms, Mol. Simul. 8 (3–5) (1992) 165–178.
[43] Y.C. Wang, S. Abe, S. Latham, P. Mora, Implementation of particle-scale rotation in the 3-D lattice solid model, Pure Appl. Geophys. 163 (2006) 1769–1785.
[44] N.V. Brilliantov, T. Pöschel, Kinetic Theory of Granular Gases, Oxford University Press, 2004.